PROCEEDINGS, 46th Workshop on Geothermal Reservoir Engineering
Stanford University, Stanford, California, February 16-18, 2021
SGP-TR-218

Numerical Simulation of Injection Tests at Utah FORGE Site

Pengju Xing[1], Branko Damjanac[2], Zorica Radakovic-Guzina[2], Aleta Finnila[3], Robert Podgorney[4], Joseph Moore[1], John McLennan[5]

1 Energy & Geoscience Institute, University of Utah, Salt Lake City, UT, USA

2 Itasca Consulting Group, Inc., Minneapolis, MN, USA

3 Golder Associates, Redmond, WA, USA

4 Idaho National Laboratory, Idaho Falls, ID, USA

5 Department of Chemical Engineering, University of Utah, Salt Lake City, UT, USA

Keywords: Numerical simulation, Pressure history matching, Hydraulic fracture, DFN, FORGE

ABSTRACT

In 2017 and 2019, injection testing was carried out in three zones in Well 58-32, drilled into granitic rock at the Frontier Observatory for Research in Geothermal Energy (FORGE) site near Milford Utah. Some of the injection tests were simulated numerically with a distinct element method (DEM) based code - XSite™, which is a fully coupled hydro-mechanical model with explicit representations of discrete fracture network (DFN). The 3D DFN contains more than 1000 natural fractures. The objective of these back analyses is to calibrate the model with respect to unknown and uncertain in situ reservoir parameters and to match the recorded pressure histories. Of particular interest are the increasing trends in the injection pressure histories and their relative magnitudes in Cycles 4 and 5, conducted in a perforated section of the cased well. The pressures measured during Cycle 5 exceeded those recorded during an identical injection stage (Cycle 4) pumped earlier in the same perforation cluster. The numerical analyses show that the interaction of the hydraulic fracture and 3D DFN, and response of DFN to fluid flow and dissipation are vital to understanding the injection pressure performance. The location, size, and properties of natural fractures significantly affect the injection pressure. The numerical study shows that the increasing pressure trends are due to fluid diversion into the DFN as localized leakoff and deformation (including slip and dilation) of the DFN. The higher pressure in Cycle 5 is mainly the result of irreversible deformation by fluid injection in the previous test (Cycle 4). The numerical investigation enhances our understanding of the FORGE reservoir. It sheds light on what might be called self-shadowing, where one injection cycle impacts the injection performance of a subsequent stage pumped at the same location.

1. INTRODUCTION

In 2017, Well 58-32 was drilled vertically to a depth of 7536 ft at the Utah Frontier Observatory for Research in Geothermal Energy (FORGE) to characterize subsurface temperatures, lithologies and permeabilities. In 2017, a series of injection tests were conducted in the uncased barefoot section of the well from 7375 to 7525 ft measured depth (MD), denoted as Zone 1. In 2019, a second series of tests were conducted in Zone 1 and in the cased and perforated portions of the well at depths of 6964 – 6974 ft MD, and 6565 – 6575 ft MD, respectively (Zone 2 and Zone 3). Up to nine test cycles were conducted in each zone. Descriptions of the injection activities and in-situ stresses and permeability interpretations from these pump-in/shut-in or pump-in/flowback tests are well documented in Xing et al (2020a) and Xing et al (2020b). Two tests, Cycle 4 and 5 were conducted in the lower cased section of the well (Zone 2), where the formation contains abundant pre-existing joints critically oriented for slip. These two injection cycles were selected for back analysis and history pressure matching. Injection pressure histories during both cycles show a monotonously increasing trend, and the pressures in the second test (Cycle 5) are consistently greater than those during the first test (Cycle 4). The purpose of the back analysis was to understand the mechanisms resulting in the trends observed from the field data, validate the numerical model by qualitatively reproducing the data trends, and calibrate the model with respect to unknown and uncertain input parameters by improving the quantitative match between numerical results and the field data.

The back analysis was conducted using *XSite* (Itasca Consulting Group, 2020), a numerical software for simulation of hydraulic fracturing in naturally fractured reservoirs. The code, which implements the synthetic rock mass (SRM) method in lattice (Damjanac et al., 2020), can simulate propagation and interaction of multiple hydraulic fractures and pre-existing joints. Hydraulic fractures propagate as a combination of predominantly tensile fracturing through intact rock at the fracture tip and opening and slip of pre-existing joints.

In this paper, the data from Cycles 4 and 5 from Zone 2 in Well 58-32 are presented first. The model input parameters are reviewed, including granitic reservoir's hydro-mechanical properties, the discrete fracture network (DFN), fluid properties, and in-situ conditions. The model results are presented and discussed, including the relevant insights learned from the back analysis.

2. INJECTION TESTS

2.1 Description

Well 58-32 was drilled to 2297 m (7536 ft) and plugged back to 2294 m (7525 ft) MD RKB (rotary kelly bushing), penetrating more than 1372 m (4500 ft) of granite. As shown in Figure 1, the well encountered low permeability crystalline rocks at a depth of 968 m (3176 ft) MD RKB and a bottom-hole temperature of 199°C (390°F).

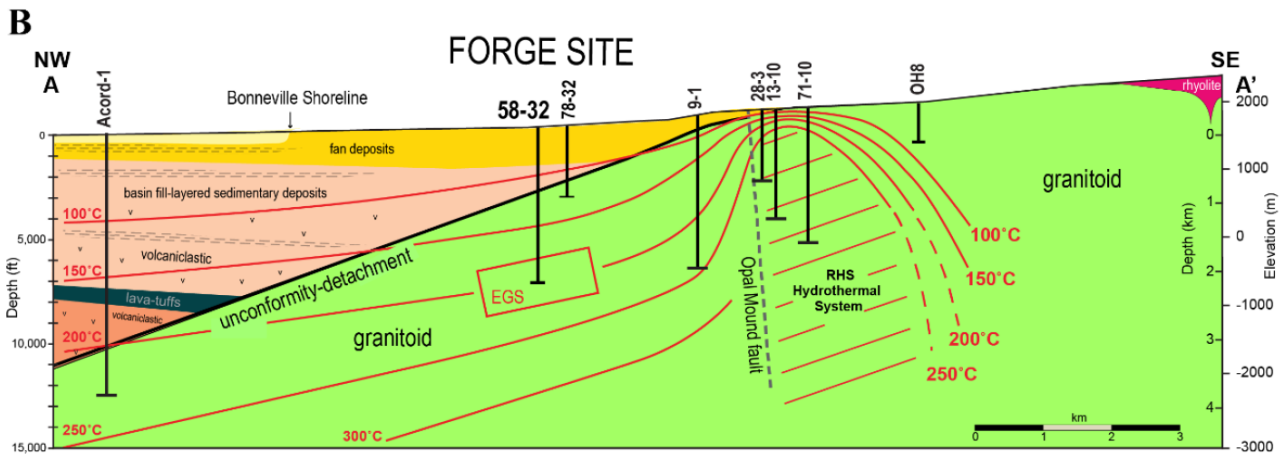

Figure 1. Northwest-southeast section through the FORGE site (adapted from Kirby et al, 2018).

In each zone, a program of up to nine injection cycles was conducted. Zone 2 was perforated over a 3.05 m (10 ft) interval from 2123 to 2126 m (6964 to 6974 ft) MD. The guns were loaded with 30-gram charges at six shots per foot and 60° phasing. Gradients were calculated using 2122 m (6961 ft) TVD (true vertical depth) RKB. This zone was picked for an injection test because it contained abundant pre-existing fractures (determined from the FMI, formation micro-imager that had been run before casing in 2017) that were estimated to be almost critically stressed and prone to shear and dilation.

During Cycle 4 for Zone 2, water was pumped for approximately six minutes at 1.32×10^{-2} m^3/s (5 bpm). The pumped volume was 5.1 m^3 (32 bbl). Subsequently, the well was shut-in for 20 hours. There was no flowback during shut-in after Cycle 4. During Cycle 5 for Zone 2, water was pumped again for six minutes at 1.32×10^{-2} m^3/s (5 bpm). The total volume of water pumped was 5.1 m^3 (32 bbl). The well was shut-in for 10 minutes after Cycle 5 pumping, during which time there was a pressure drop to 17.8 MPa (2,580 psi). Subsequently, flowback was allowed through a 1/64-inch choke after approximately 20 minutes. Next, the choke was beaned up by 1/64 inch every 5 minutes until it was fully open. The pressure drop after one hour was too small to measure, similar for flow. The total recovered water was 2.8 m^3 (17.6 bbl). After the well was shut in again, the pressure built to 0.89 MPa (130 psi). The comparison of injection parameters for Cycle 4 and 5 are summarized in Table 1.

Table 1 Injection parameters for Cycle 4 and 5, Zone 2

Parameter	Cycle 4	Cycle 5
Pumping rate	5 bpm	5 bpm
Pumping time	6 min	6 min
Pumping volume	32 bbl	32 bbl
Surface pressure at the end of injection	3700 psi	3925 psi
Shut-in time	20 hr	10 min
Flowback operation	No	Yes

The injection rate and pressure histories for Cycle 4 during pumping and the early portion of the shut-in are shown in Figure 2. Notice that, since the packer failed, a dead string (annulus between tubing and casing) was recording a slightly lower pressure than the tubing because there is no friction in that static fluid space. The pressure history exhibits an early peak corresponding to breakdown (i.e., fracture initiation from the perforations and coalescing into a vertical hydraulic fracture perpendicular to the minimum horizontal principal stress). After the pressure drop following the breakdown, the pumping pressure increases steadily.

Lack of the early peak in the pumping pressure history during Cycle 5 (shown in Figure 3) from the same perforation cluster was expected because the hydraulic fracture had already been created in Cycle 4. The pumping pressure during Cycle 5 monotonically increases for the entire duration of the pumping, as occurred during Cycle 4. Another interesting observation when the pumping pressures from Cycles 4 and 5 are compared (Figure 4) is that the pressure during Cycle 5 is greater than during Cycle 4.

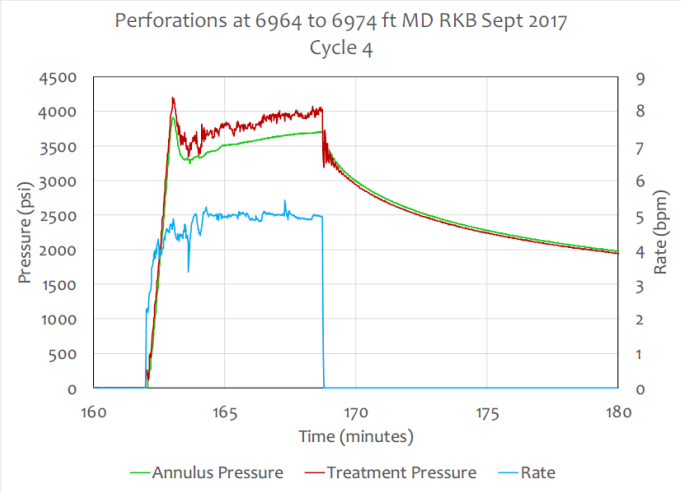

Figure 2 Injection rate and pressure histories for Zone 2, Cycle 4 showing pumping and the early portion of shut-in.

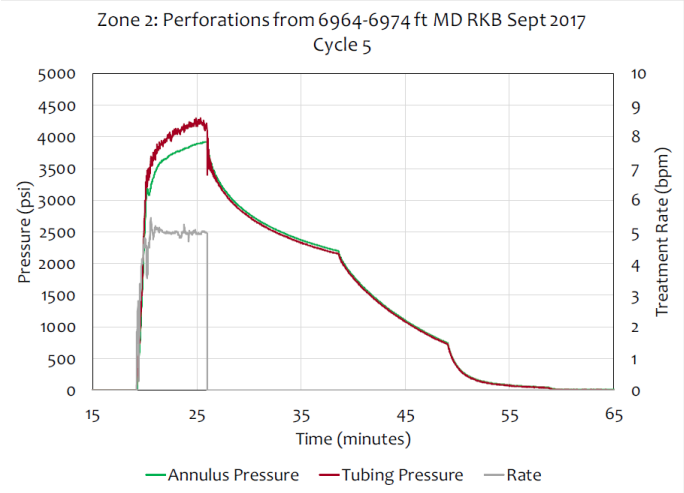

Figure 3 Injection rate and pressure histories for Zone 2, Cycle 5 showing pumping and complete shut-in and flowback.

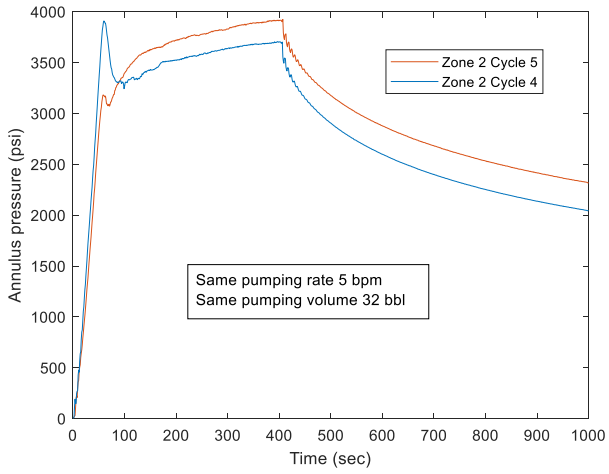

Figure 4 Comparison of pressure histories between Cycles 4 and 5 in Zone 2 during pumping and the early portion of shut-in.

2.2 Discussion

There are a couple of interesting observations from the data recorded during these two injection tests. In both tests (after breakdown in Cycle 4), the injection pressure steadily increases for the duration of the pumping. Injection into a perforation cluster in a homogeneous

continuous medium is expected to propagate a penny-shaped hydraulic fracture perpendicular to the minimum principal stress. The injection pressure in that case is also expected to decrease steadily. The increasing pumping pressure would be expected if:

- the fracture height is limited (e.g., the fracture is contained, usually by a stress barrier, within a layer of relatively small thickness);
- there is sufficient leakoff into the surrounding formation, resulting in a poro-elastic effect (due to increase in total stress); or
- the hydraulic fracture interacts with pre-existing joints, which are arresting its tip and/or diverting fluid into the fracture network (as localized leakoff).

Based on the overall geology as well as the stiffness, and permeability of the granite, determined from the tests conducted on core samples and logging, it seems that interaction of the hydraulic fracture with the DFN is the most plausible explanation for increasing pumping pressures.

Greater pumping pressures during Cycle 5 compared to Cycle 4 are a consequence of irreversible or slowly (compared to 20 hours of shut-in) evolving changes induced by fluid injection into fractures in the surrounding formation. The permeability changes resulted from pumping during Cycle 4 are associated with fracture creation and opening and slip of pre-existing fractures. With dissipation of fluid pressure, fractures that were created and opened will close. This process is certainly partially reversible. However, it might not be completely reversible because of the fracture surfaces' roughness and potential shear deformation preventing complete closure of mismatched fracture surfaces. Slip on rough fractures will result in a mostly irreversible increase in aperture (dilatancy) and permeability. However, if the increase in permeability affects subsequent pumping in the same cluster, that effect would be reduction in the injection pressure, which is opposite to the pumping data (showing increased pressures in the subsequent injection).

The other long-term transient or irreversible change caused by fluid injection is the increase in the mean stress around the injection point due to a poro-elastic effect by which the increase in pore pressure in the matrix and/or pre-existing fractures results the total stress increase. If the induced fluid (pore) pressure does not dissipate before the subsequent injection, the confining stresses will be greater, resulting in greater pressures during subsequent injection(s). However, because of small hydraulic diffusivity and a small conventionally defined Biot's coefficient for intact granite, this effect cannot be significant in the matrix during the tests at Zone 2. Although the fluid pressure is expected to dissipate into the pre-existing joints during injection, a relatively long shut-in period should be sufficient to dissipate the pore pressures. A possible exception might be if fracture closure during dissipation results in a pinching effect, leaving relatively large fluid pressures trapped around the injection point. This mechanism is not likely because the pressure history data indicate an expected dissipation of fluid pressure. Thus, the most likely mechanism that can explain an increased injection pressure during the second test (Cycle 5) is an irreversible stress change caused by irreversible deformation, specifically slip on the pre-existing DFN. Slip on pre-existing fractures, particularly if associated with dilatancy, will increase volume and hence increase in total stresses under confined conditions, requiring greater pressure to reopen the fractures. The increase of the total stresses resulted from irreversible deformation outweighed the effect of the permeability increase, thus making injection pressure higher in the subsequent cycle (Cycle 5).

The numerical model used for the back-analysis and pressure matching was setup considering the possible mechanisms. The DFN was explicitly represented in the model, and the DFN's initial apertures and permeability in the model were calibrated in this exercise. Based on hydraulic and thermal diffusivities and the relatively short duration of the injections, it was assumed that matrix leakoff and thermal effects were second-order effects on the test results. Leakoff into the DFN was explicitly represented.

3. NUMERICAL MODEL

3.1 Input Parameters

The mechanical properties of the granite, as listed in Table 2, were determined from the laboratory experiments on core samples from the well. Those properties were assigned to the entire rock formation in the model. Fluid viscosity is assumed to be 1.13×10^{-3} Pa×s (1.13 cP).

Table 2 Rock Properties

Parameter	Value
Young's modulus	50 GPa (7.25×10^{6} psi)
Poisson's ratio	0.25
Fracture toughness	1.75 MPa×$m^{1/2}$ (1600 psi×$in^{1/2}$)
Permeability	10^{-17} m^2 (10^{-2} mD)
Porosity	0.01

Four different DFN realizations shown in Figure 5 were generated with varying numbers of fractures and sizes. As shown in the upper left of Figure 5, the simplest DFN has only one steeply dipping (65°) fracture with a dip direction of N125°E (i.e., the normal at a small angle relative to the orientation of the minimum principal stress, N115°E). Within Zone 2, that fracture was explicitly mapped and is

critically oriented for slip relative to the principal stresses. However, its dimensions are uncertain. In these simulations, it was assumed that the radius of the fracture is 50 m. That fracture is included in all four DFNs. Most of the simulations discussed in this study were conducted using the model with 1992 DFN fractures (lower right of Figure 5). Some simulations were carried out with a smaller scale model with only five fractures. The purpose of the small-scale model was to investigate in more detail interactions between hydraulic fracture and natural fractures, particularly considering uncertainties in DFN strength and dilatancy.

These DFNs were simplified from the FORGE Reference DFN (Finnila et al., 2019) to allow their explicit representation in the numerical models without affecting model accuracy (and the effect of the DFN on model results), size, or execution time (i.e., the run time). The two main simplifications were:

- the minimum fracture radius is 10 m; and
- the DFN includes three fracture sets with different orientations. However, all fractures within each set have the same strike (i.e., there is no variation in fracture orientation within a single set).

In most of the simulations, it was assumed that the pre-existing fractures are frictional, with a 37° friction angle. The initial fracture apertures are correlated with fracture sizes. Selecting the variability of the initial apertures ranging between 4 and 10 μm (as shown in Figure 6) appears to yield the best pressure history matching.

The pore pressure and initial stress conditions are listed in Table 3. In the model, it was assumed that the stress and pressure variations due to in-situ gradients are not significant over the height of the domain affected by fluid injection. Therefore, the uniform stresses and pore pressures were initialized in the model.

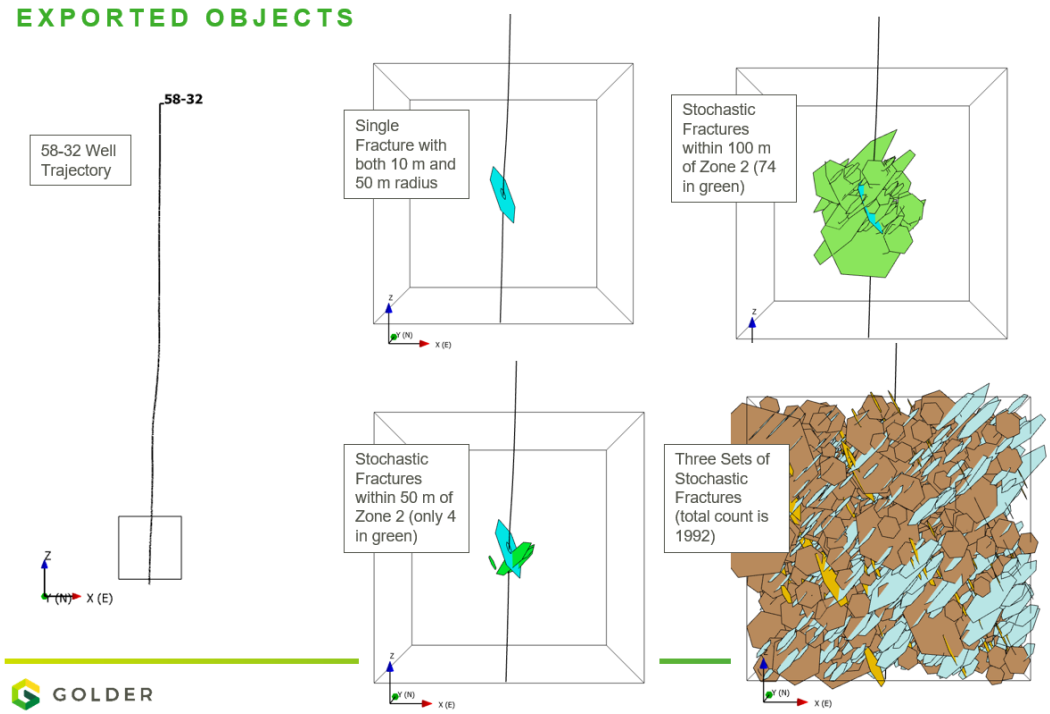

Figure 5. DFNs included in the models.

Table 3 Initial Conditions

Variable	Gradients	Magnitudes in Zone 2
Pore pressure	0.0097 MPa/m (0.43 psi/ft)	20.8 MPa (3014 psi)
Minimum horizontal stress	0.017 MPa/m (0.77 psi/ft)	37.0 MPa (5360 psi)
Maximum horizontal stress	0.0199 MPa/m (0.88 psi/ft)	42.2 MPa (6126 psi)
Vertical stress	0.0256 MPa/m (1.13 ft/ft)	54.2 MPa (7866 psi)

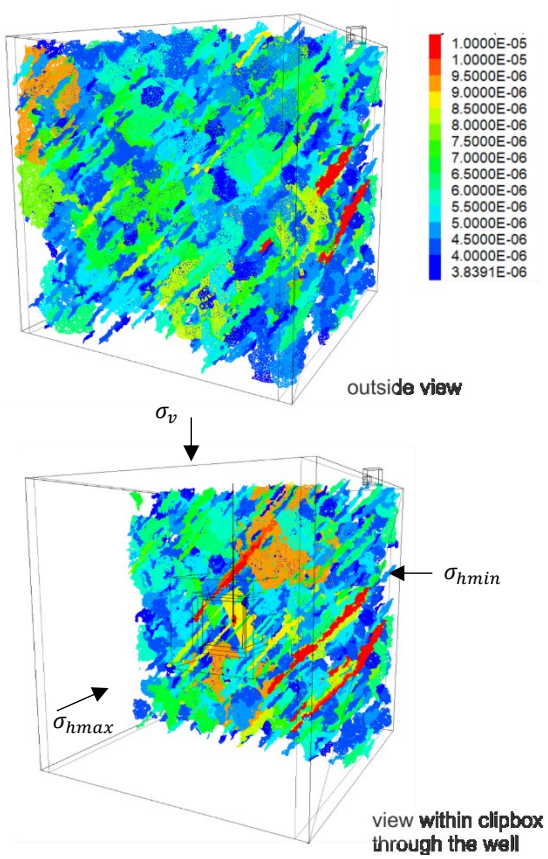

Figure 6. Initial DFN apertures (m).

3.2 Description

The large-scale model with 1992 DFN fractures has a cubic shape with an edge length of 300 m. This boundary dimension was selected so that fluid pressure and stress perturbations due to injection are relatively small at the model boundaries. These are truncation boundaries facilitating the use of a finite-size model to represent processes taking place in an infinite half-space. The outside boundaries have "rollers" in the mechanical model and are impermeable in the fluid flow model. The model is set up to simulate fracture propagation but not fracture initiation, because an attempt to capture very different time and length scales, fracture initiation and propagation, in the same model would make it excessively large and slow to execute. Therefore, the borehole and the perforations are not explicitly modeled. In the model, the hydraulic fracture starts propagation from a small start-up penny-shaped fracture perpendicular to the minimum principal stress (i.e., it is assumed that the hydraulic fracture was already initiated).

The simulation was carried out in steps. Mechanical equilibrium was achieved first for the initial stress and pore pressure conditions. Some readjustment of stresses took place as a result of the explicitly represented DFN. Subsequently, the injection tests were simulated as fully coupled hydro-mechanical processes, including Cycle 4, shut-in for 20 hours, and Cycle 5.

3.3 Parametric Study with A Small-scale Model

Before investigating the large-scale model with 1992 natural fractures, it was desirable to conduct a sensitivity study in a small-scale model. The interaction between the hydraulic fracture (HF) and the DFN was investigated in more detail using a 100 m-edge cube model (with only five fractures as shown in Figure 7) with finer resolution. This sensitivity study investigated the modes of interaction (i.e., crossing and arrest) as a function of fracture parameters, including friction angle, tensile strength, cohesion, and dilation angle.

Figure 7 through 9 depicts the effect of natural fracture (DFN) tensile strength and cohesion, friction angle, and dilatancy on HF and DFN interactions. As shown in Figure 7, when the DFN fracture is strong with high tensile strength and cohesion, the HF crosses the closest fracture from the critically oriented DFN set. On the other hand, when the DFN fracture is weak with a relatively small tensile strength and cohesion, the HF is arrested by the DFN. This suggests that the DFN tensile strength needs to be very high to promote crossing. Visual inspection of the core indicates that the natural fractures likely do not have excessive tensile strength or cohesion. In the large-scale model, the DFN tensile strength and cohesion are both defined assumed to be zero, and therefore the initiating hydraulic fracture is prone to be arrested by DFN.

The friction angle from experiment on core samples ranges between 30° and 50°. The results of bounding values of the friction angle are shown in Figure 8. In both cases, the HF is arrested by the DFN. However, in the high friction angle case, fluid pressure in the DFN is higher and the HF is shorter. The reason for this behavior is that with higher friction angles, higher pressure is required to make the DFN fail in shear. At the same time higher pressure promotes the DFN fracture opening, resulting in more fluid leaking into the DFN and forming a shorter HF.

(a)

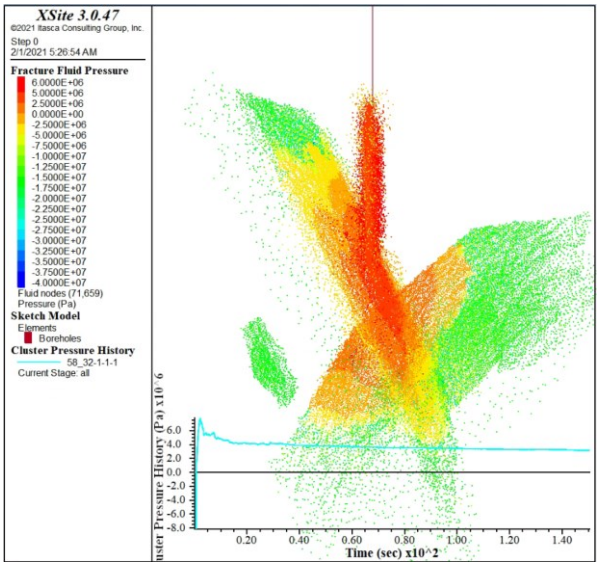

(b)

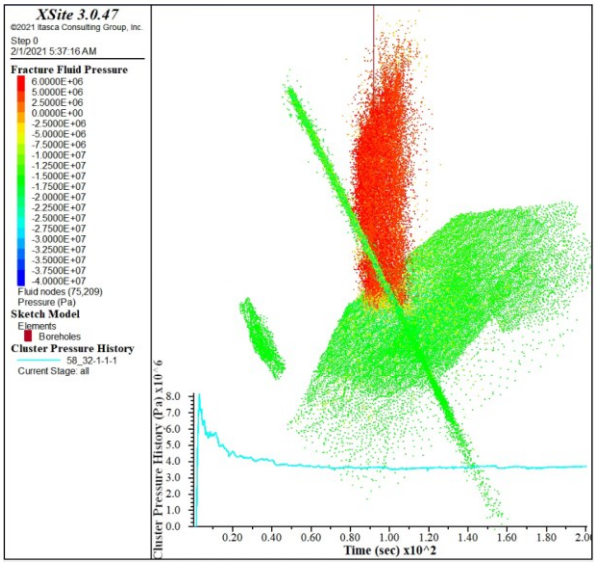

Figure 7. Effect of DFN tensile strength and cohesion on interactions of HF and DFN. (a) The HF is arrested by the DFN with a 37° friction angle, 0 MPa tensile strength, and 0 MPa cohesion. (b) The HF crosses the natural fracture with a 37° friction angle, 20 MPa tensile strength, and 20 MPa cohesion.

Figure 9 shows the effect of dilatancy on HF and DFN interactions. In Xsite, aperture increase due to dilation is given by

$$\Delta d_n = \Delta d_s \tan \phi_{dil} \tag{1}$$

where Δd_n is fracture aperture increase due to dilatancy, Δd_s is slip distance, and ϕ_{dil} is dilation angle. For the case with 2° dilation angle, the DFN fails in shear under compressive effective stress. The DFN fracture aperture increase due to the dilatancy forms a high permeability channel that increases fluid leakoff into the DFN. Also, the HF is arrested after intersecting the first DFN fracture because fluid is diverted and flow into the relatively permeable DFN fractures.

The study shows that arrest is expected for a reasonable range of strengths of DFN, e.g. relatively low tensile strength and cohesion, and a friction angle below 50°. It also appears that DFN dilatancy has a profound effect on the interactions. Even a small dilatancy causes arrest of the HF and diversion of fluid into and within the DFN.

(a)

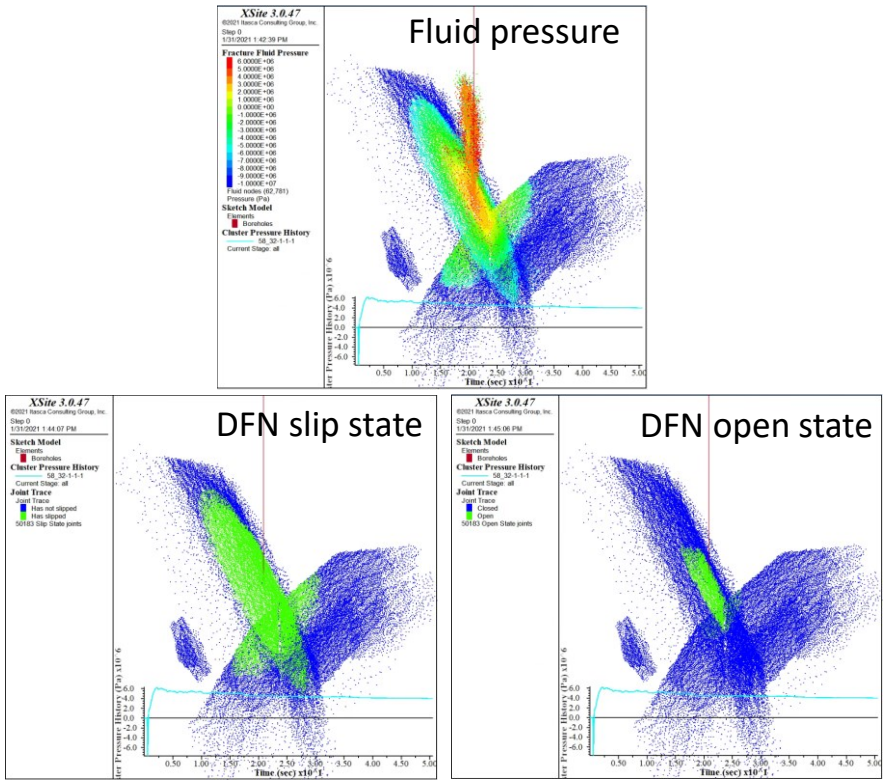

(b)

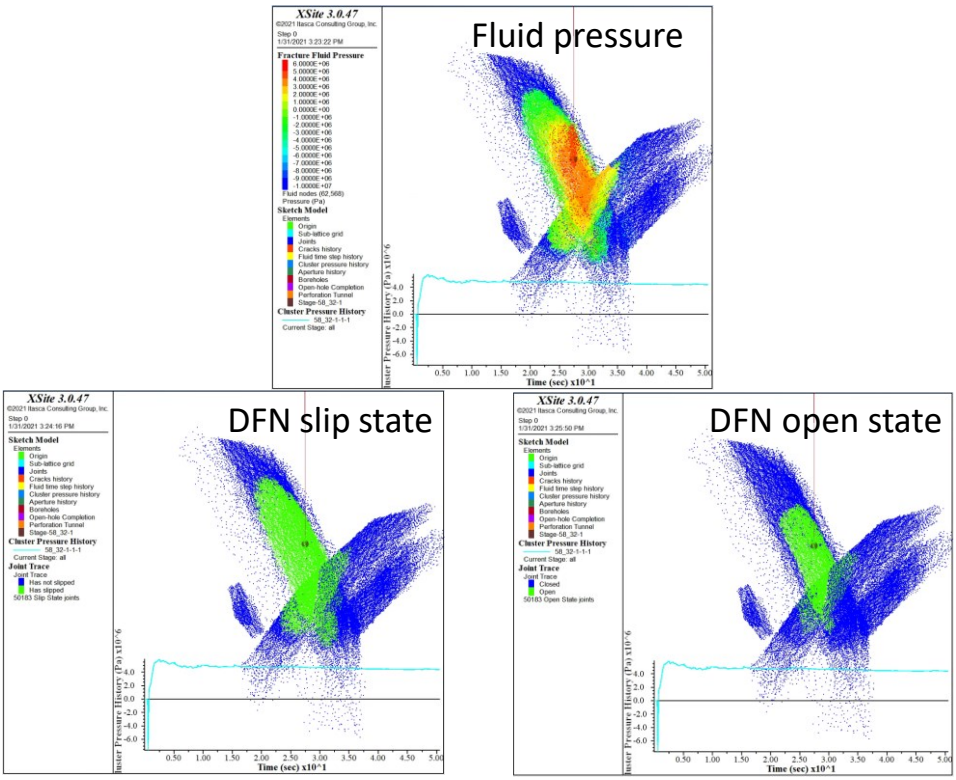

Figure 8. Effect of DFN friction angle on interactions of HF and DFN. (a) The HF is arrested by the DFN with a 30º friction angle, 0 MPa tensile strength, and 0 MPa cohesion; (b) The HF is arrested by the DFN with a 50º friction angle, 0 MPa tensile strength, and 0 MPa cohesion. A relative longer HF is created with smaller friction angle (30º) than the case with larger friction angle (50º).

(a)

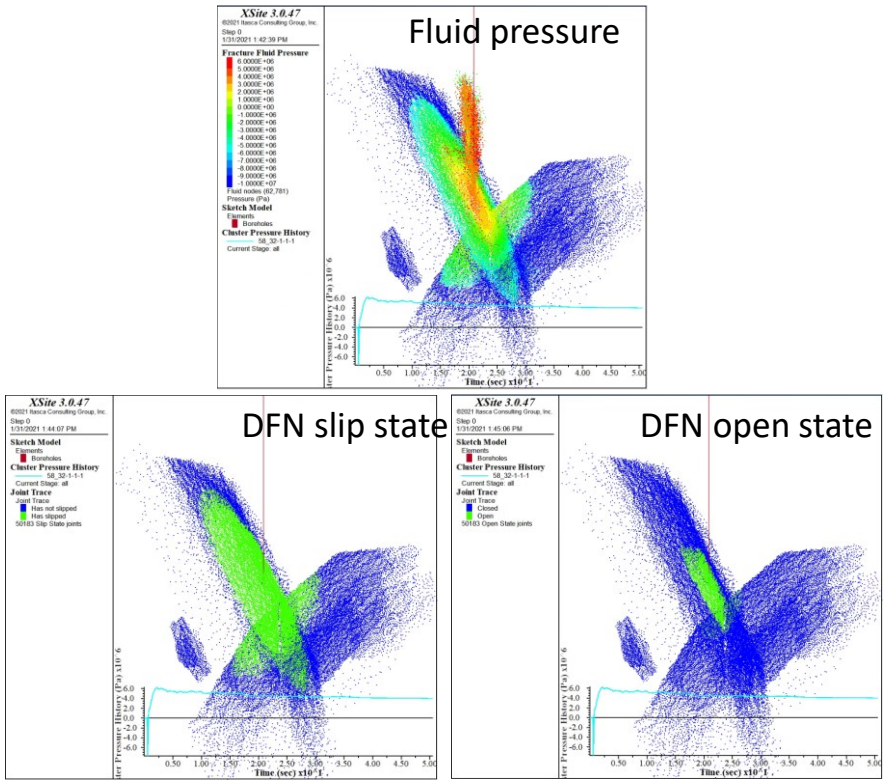

(b)

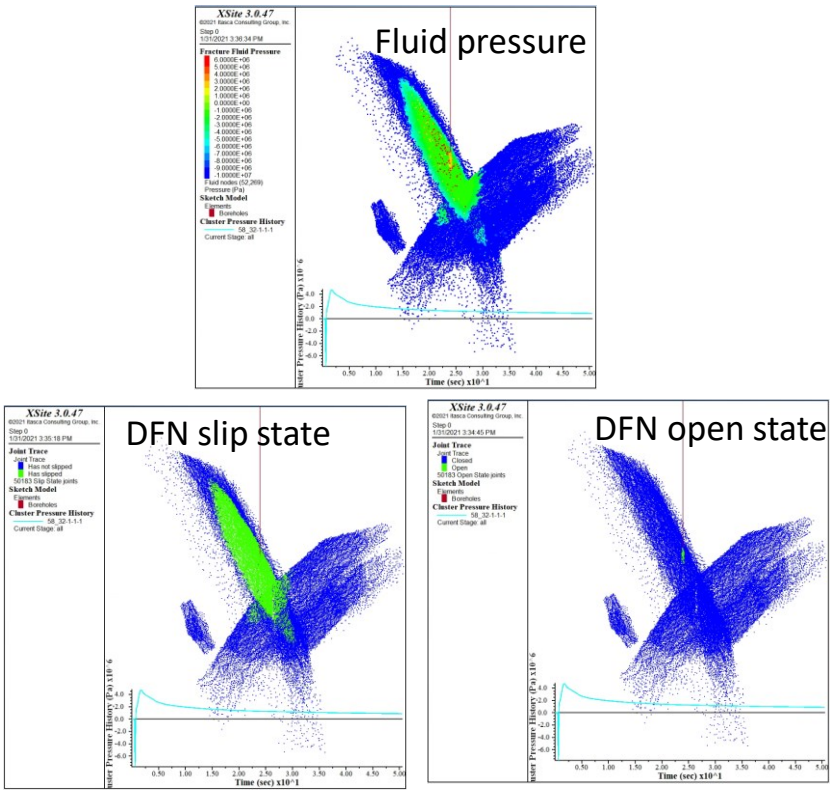

Figure 9. Effect of DFN dilation angle on interaction of HF and DFN. (a) The HF is arrested by the DFN with a 30º friction angle, 0 MPa tensile strength, 0 MPa cohesion, and no dilation; (b) The HF is arrested by the DFN with a 30º friction angle, 0 MPa tensile strength, 0 MPa cohesion, and 2º dilation angle.

3.4 Results of Large-scale Model

Figure 10 shows the injection pressures from two models, one assuming non-dilatant pre-existing DFN fractures and the other with dilatant fractures characterized by a 2° dilation angle, compared with the pressure history recorded during Cycle 4. The initial pressure peak (i.e., the breakdown pressure), probably resulting from fracture initiation, is not captured in the model results because the model did not have sufficient resolution and used a small startup joint through the perforation cluster to represent the already initiated HF. Both models qualitatively match the general increasing trend in the injection pressure history. However, the case with assumed non-dilatant joints seems to be a better match of the magnitude of the injection pressure increase during Cycle 4. The pressure increase in the model with dilatant joints is smaller because joint dilatancy results in greater fracture aperture and permeability. However, the model with dilatant fractures better matched pressures after shut-in as shown in Figure 11. Therefore, this model was used for simulation of both Cycles 4 and 5.

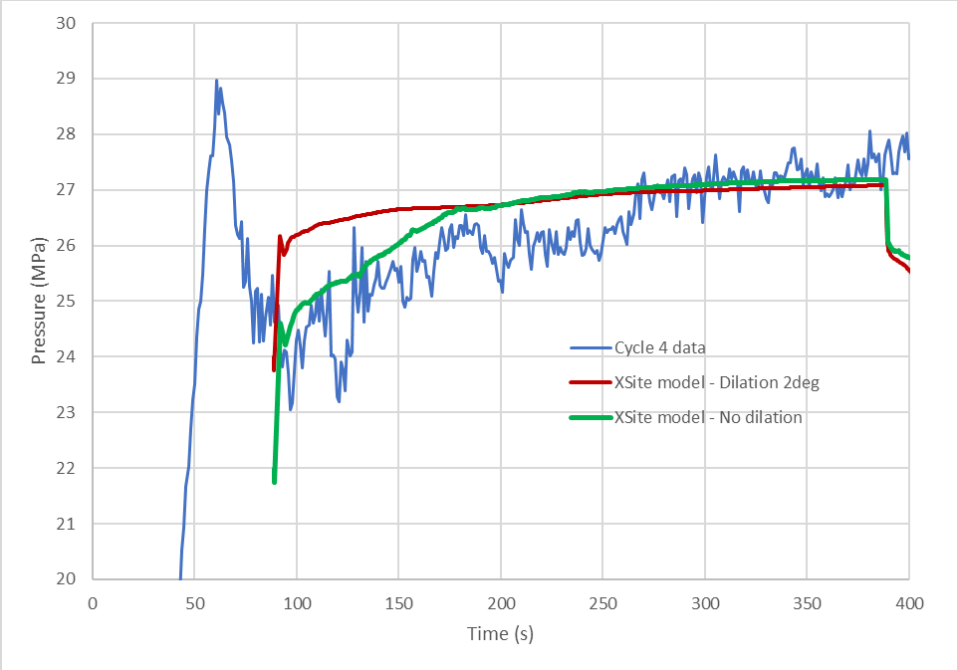

Figure 10. Cycle 4: Pressure history matching during injection.

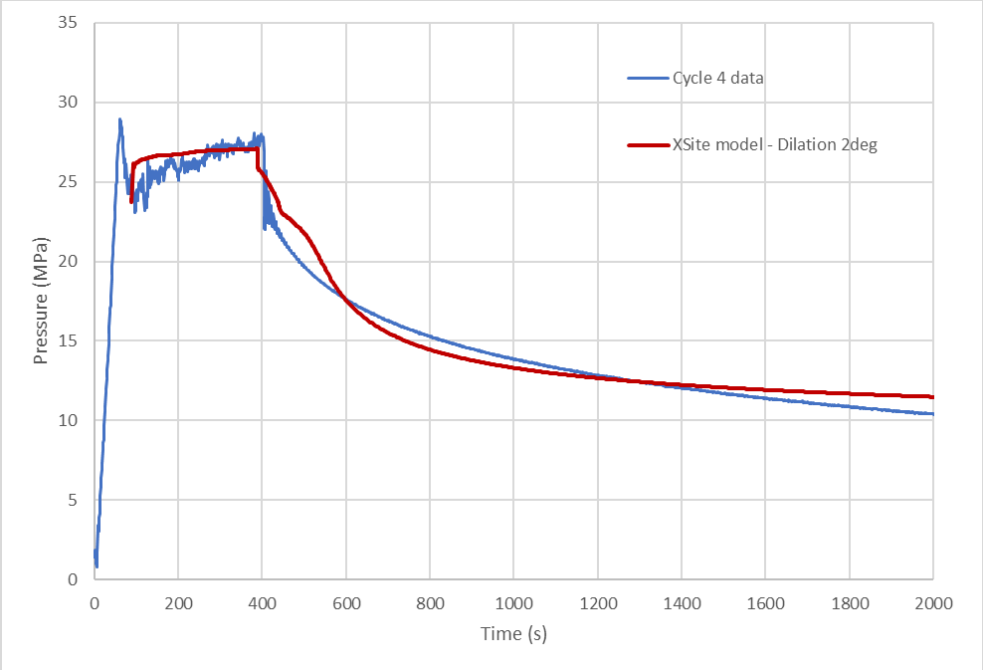

Figure 11. Cycle 4: Pressure history matching during injection and initial shut-in.

For the model with dilatant fractures (2° dilation angle), the contours of net pressure (the pressure in excess of the minimum principal stress) and the fracture apertures at the end of injection of Cycle 4, the end of the shut-in period (e.g., before Cycle 5), and the end of injection of Cycle 5 are shown in Figures 12 and 13, respectively. The results indicate that the formation response to the injection is dominated by the fluid flow and pressure dissipation in the DFN and, in particular, the pre-existing fracture from the critically oriented set close to the perforation cluster (refer to Figure 12). As shown in Figure 12, the HF is arrested by the pre-existing fracture and does not propagate a large distance from the perforation cluster, which is consistent with results from the small-scale model. The plot of aperture contours in Figure 13 illustrates the localization of deformation along the closest DFN fracture from the critically oriented set. The indicators of slip shown in Figure 14 (shown only at the end of injection of Cycle 4 because the slipping extent does not change during shut-in or Cycle 5) confirm that slip and fracture dilation (along the closest fracture from the critically oriented set) are the leading causes for localization of deformation and increase in aperture.

The recorded data and simulated (for the case with a 2° dilation angle for the DFN) pressures from Cycles 4 and 5, are compared in Figure 15. The model results match the important data trends. The injection pressure generally increases with time in both cycles. Also, the injection pressures during Cycle 5 are continuously greater than during Cycle 4. The explanation for increased injection pressure in Cycle 5 in the numerical model is illustrated in Figure 16, which, for states before Cycles 4 and 5, shows block contours (5-m edge length cells) of the change in the minimum principal stress relative to the initial far-field state. Before Cycle 4 (the top plot in Figure 16), there is no stress change except for relatively localized perturbations around the pre-existing fractures. The contours before Cycle 5 (the bottom plot in Figure 16) show an irreversible increase in the confining stress in the volume of the rock mass around the injection cluster even after dissipation of injection-reduced fluid pressures. The increase is caused by irreversible (slip related) deformation of the DFN resulting from an increase in the fluid pressure during injection.

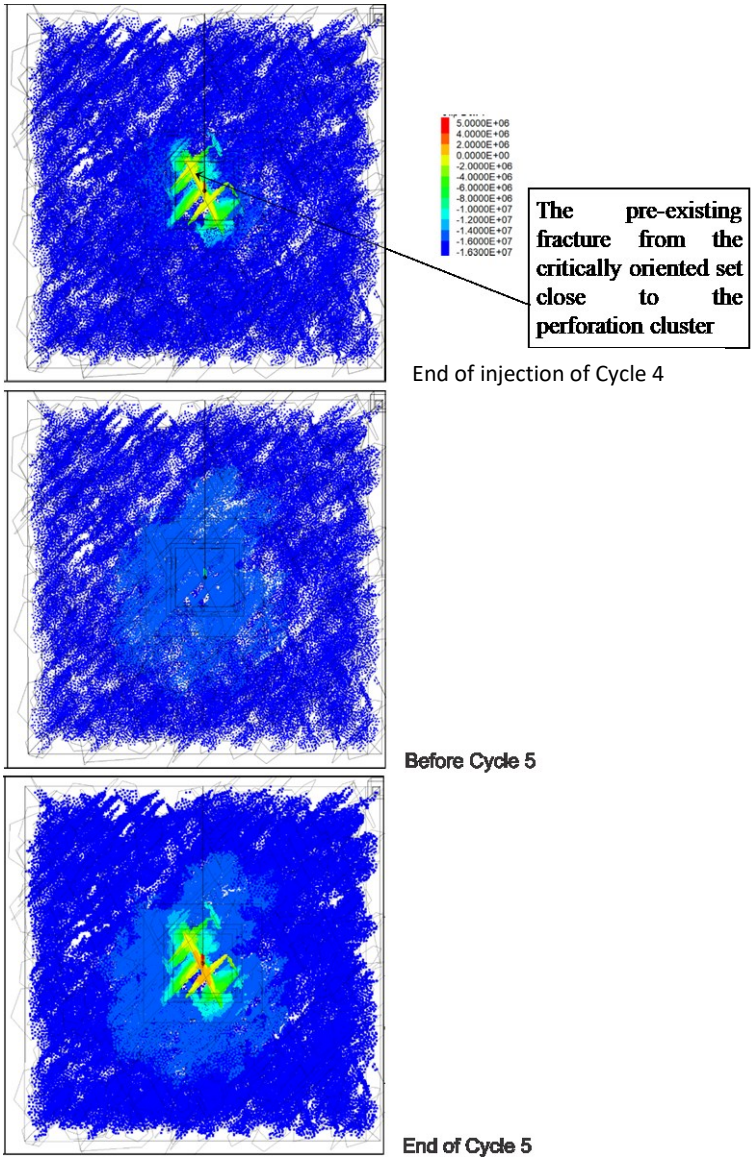

Figure 12. Fluid pressure contours (Pa) at characteristic times during injection tests in Zone 2.

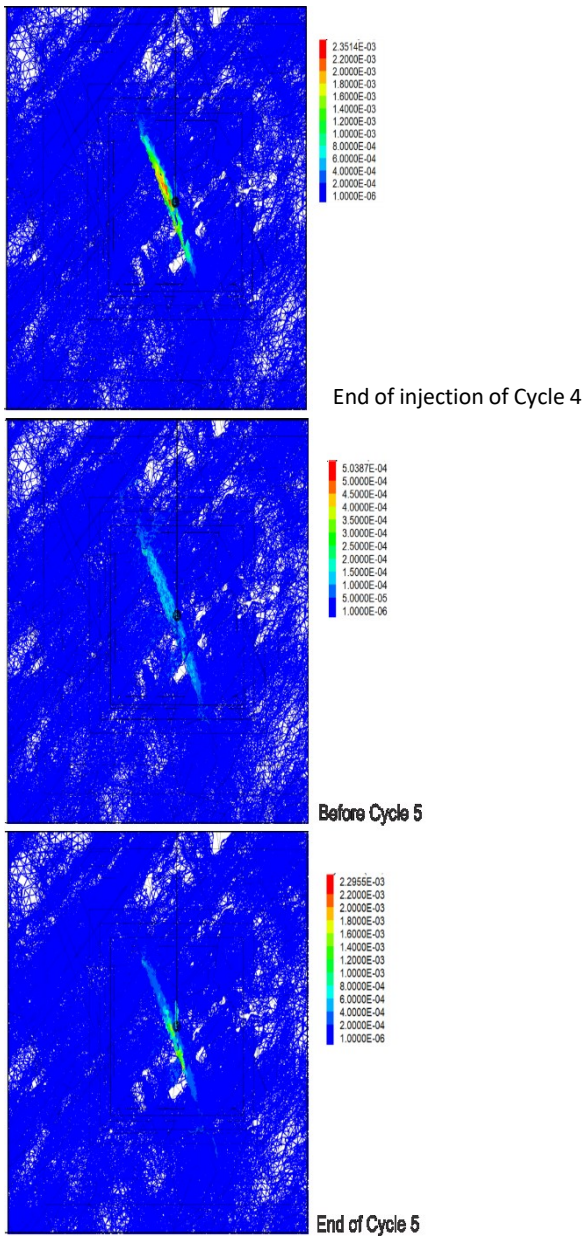

Figure 13. Fracture aperture contours (m) at characteristic times during injection tests in Zone 2.

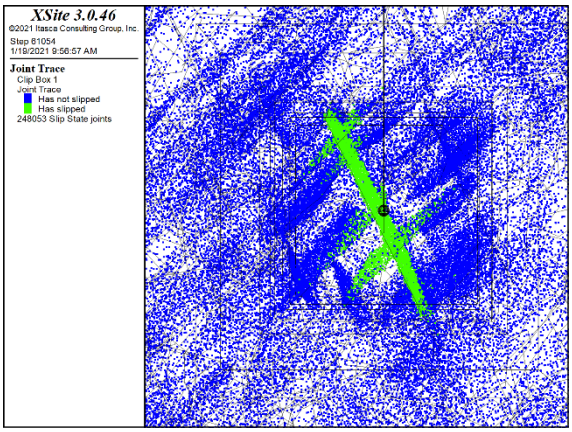

Figure 14. Indication of fracture slippage at the end of injection of Cycle 4.

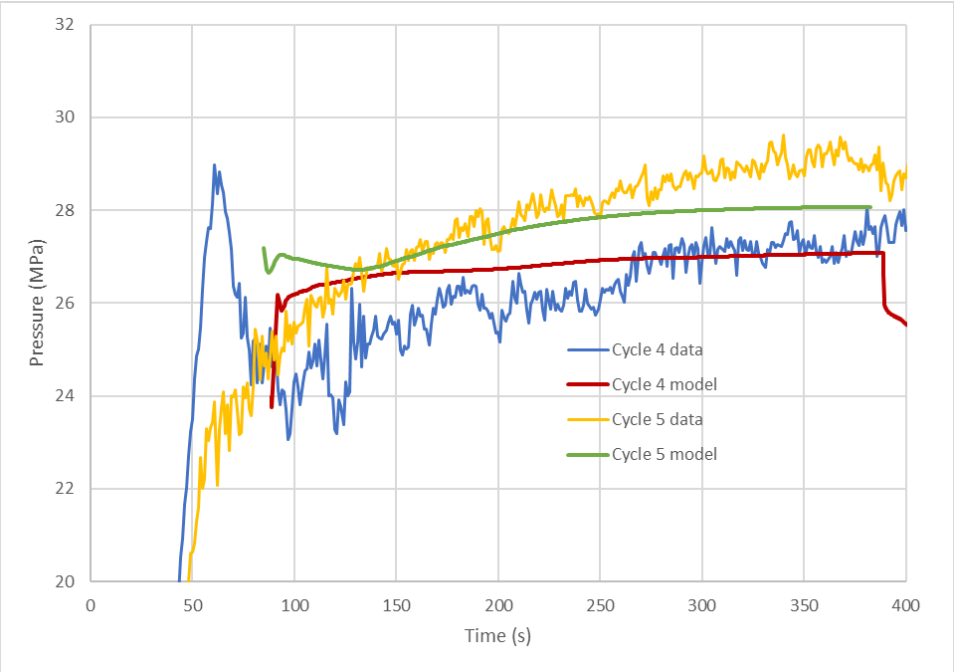

Figure 15. Cycles 4 and 5: Pressure (surface pressure) history matching during injection.

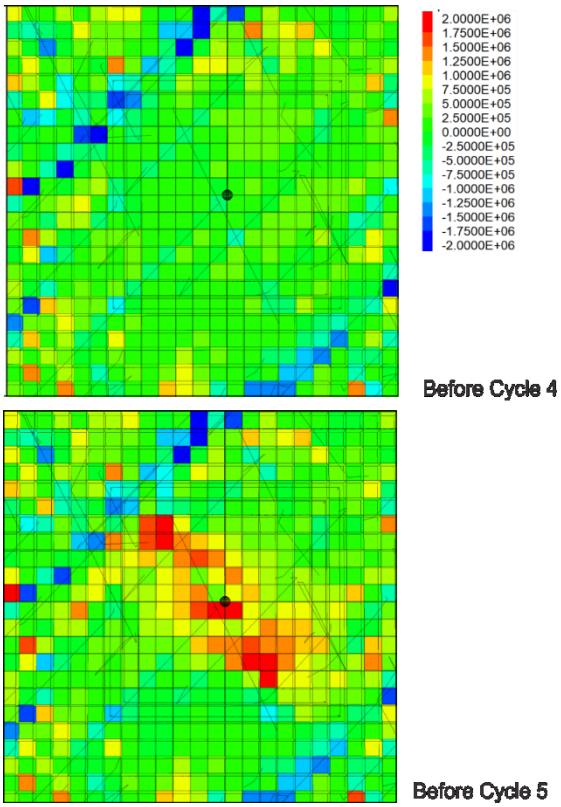

Figure 16. Contours of the change in the minimum horizontal stress (MPa) relative to the initial far-field state in the cross-section through the well, perpendicular to the maximum horizontal principal stress (refer to Figure 6).

4. CONCLUSIONS

Injection tests were conducted in perforated intervals in Well 58-32 at the FORGE site to evaluate the possibility of stimulating fractures behind casing. Clear evidence of fracture opening was observed in the lower perforated zone (Zone 2, 6964 – 6974 ft MD) during the fourth of nine injection cycles. In this study, pressures from Cycles 4 and 5 were history matched to characterize the fracture behavior.

Cycle5 was initiated after 20 hours of leakoff and shut-in. The back-analysis of Cycles 4 and 5 in Zone 2 in Well 58-32 and pressure matching indicate that the response of the formation to fluid injection is dominated by fluid flow and deformation (opening and slip) of the pre-existing fractures. The hydraulic fracture is arrested after intersecting the closest pre-existing fracture from the critically oriented set with an average dip direction of 125° and dip angle of 65°. The critical factors causing the arrest, besides the shear strength of the pre-existing fractures, are in-situ aperture and dilatant behavior, which results in a further increase in aperture (and permeability) with slip. The interaction of the relatively short hydraulic fracture with the DFN and localization of flow and deformation in the DFN cause an increase in the injection pressure.

Slippage on the fractures from the critically oriented set results in irreversible deformation and increased minimum principal stress after dissipation of the fluid pressure following 20 hours of leakoff during shut-in. This effect is more pronounced if fractures are dilatant. However, there is an increase in the normal stress in the direction of the initial minimum principal stress even when fracture slip is not associated with dilatancy. Thus, the subsequent injection test (Cycle 5) experienced greater “confining stress”, resulting in increased injection pressures.

REFERENCES

Damjanac, B., C. Detournay, and P. Cundall. (2020) "Numerical Simulation of Hydraulically Driven Fractures," in S. Baotang, O. Stephansson, & M. Rinne (Eds.), *Modelling Rock Fracturing Processes* (2nd ed., pp. 531–561). Springer, Cham. https://doi.org/https://doi.org/10.1007/978-3-030-35525-8

Finnila, A., Forbes, B., & Podgorney, R. (2019). Building and Utilizing a Discrete Fracture Network Model of the FORGE Utah Site. In *Proceedings of the 44th Workshop on Geothermal Reservoir Engineering, Stanford University, Stanford, CA, USA* (pp. 11-13).

Itasca Consulting Group, Inc. (2020) *XSite* (Version 3.0.47). Minneapolis: Itasca Consulting Group, Inc.

Kirby, S. M., Knudsen, T. R., Kleber, E., & Hiscock, A. (2018). Geologic setting of the Utah FORGE site, based on new and revised geologic mapping. *Trans. Geotherm. Resour. Counc*, *42*, 1097-1114.

Xing, P., Goncharov, A., Winkler, D., Rickard, B., Barker, B., Finnila, A., Ghassemi, A., Podgorney, R., Moore, J., and Mclennan, J. (2020a). Flowback Data Evaluation at FORGE. In *54th US Rock Mechanics/Geomechanics Symposium*. American Rock Mechanics Association.

Xing, P., McLennan, J., and Moore, J. (2020b). In-Situ Stress Measurements at the Utah Frontier Observatory for Research in Geothermal Energy (FORGE) Site. *Energies*, *13*(21), 5842.